Article

日本大学生産工学部研究報告 A
2026 年 6 月 第 59 巻 第 1 号

Cocrystals of Quasiracemic Square-planar Pd(II) and Pt(II) Complexes with Optically-active Schiff Base Ligands

*Masahiro IKESHITA**, *Takashi TSUNO***

(Received December 10 . 2025)

Abstract

Quasiracemates, formed from quasienantiomeric pairs of chiral metal complexes, present a platform for investigating the relationship between molecular chirality and crystal packing. We report the synthesis and single-crystal X-ray characterization of quasiracemic cocrystals composed of the square-planar Pd(II) and Pt(II) complexes (*S,S*)-**2**/(*R,R*)-**3** and (*R,R*)-**2**/(*S,S*)-**3**, bearing optically active Schiff-base ligands. Slow evaporation from CH_2Cl_2/*n*-hexane afforded red prisms, crystallizing in the chiral space group $P2_1$ with unambiguous absolute configurations, whereas the corresponding racemic crystals adopt centrosymmetric arrangements ($P2_1/c$, $P2_1/n$). Structural analysis reveals pseudo-enantiomeric packing stabilized by π – π interactions between naphthalene moieties in the ligands, closely emulating the arrangement of racemates despite differing metal centers. Coordination geometries are consistent with (*SP*-4-1)-[M(O^N)$_2$] (M = Pd, Pt) in the Cambridge Structural Database (CSD), and the difference in ionic radii between Pd(II) and Pt(II) minimally affects the chelate framework. Subtle variations in O–N–O–N torsion angles introduce a diastereomeric relationship within the quasiracemates, reflecting the structural adaptability required for quasi-mirror-image packing. This study provides a rare, rigorous comparison between racemic and quasiracemic assemblies of square-planar metal complexes and establishes guiding principles for the design of heterometallic chiral solids with controlled lattice symmetry and potential functional properties.

Keywords: Cocrystals, Quasiracemates, Quasienantiomers, Square-planar Pt(II) complex, Square-planar Pd(II) complex

1 . Introduction

Cocrystals have been extensively investigated in pharmaceutical science[1] because they can exhibit physical and chemical properties that differ markedly from those of the corresponding single-component crystals, primarily as a result of modified intermolecular interactions and molecular packing. Chiral compounds that are structurally analogous and exist as non-superimposable mirror-image counterparts are referred to as quasienantiomers.[2] Cocrystals derived from quasienantiomers, known as quasiracemates,[2),3)] provide diverse opportunities for the design of advanced functional materials, including optoelectronic,[4] spintronic,[5] energetic,[6] and mechanochromic[7] materials. In such systems, the constituent chiral molecules adopt pseudo-mirror-image arrangements that mimic racemic packing, while the crystal as a whole retains its intrinsic chirality.

Although numerous studies have focused on readily accessible amino acid– or organic compound–based cocrystals, extending this concept to cocrystals composed of dissimilar metal complexes or organometallic species

*Assistant Professor, Department of Applied Molecular Chemistry, College of Industrial Technology, Nihon University
**Professor, Department of Applied Molecular Chemistry, College of Industrial Technology, Nihon University

is expected to yield synergistic solid-state properties arising from the combined characteristics of the individual complexes. Furthermore, the incorporation of chiral organic ligands into metal complexes provides additional functionalities, including crystal engineering and distinctive chiroptical responses.

The first report of quasiracemates consisting of two structurally similar chiral metal complexes containing different metal ions appeared more than a century ago. Delépine provided the earliest documented example in 1921, describing the mixed-crystal system Δ-(–)-K_3[Ir(ox)$_3$]·Λ-(+)-K_3[Rh(ox)$_3$]·9H_2O (ox = oxalate dianion).[8] In 1930, additional quasiracemate structures formulated as [Δ-(–)-Co(en)$_3$·Λ-(–)-Rh(en)$_3$]X_6 (en = ethylenediamine; X = Cl, Br, or I), together with an isomorphous analogue [Δ-(–)-Co(en)$_3$·Δ-(+)-Rh(en)$_3$]X_6, were reported.[9] These early investigations relied solely on solution-phase optical rotation measurements; consequently, the absolute configurations of the constituent complexes remained undetermined. A decisive advance was achieved in 1969, when Andersen and co-workers assigned the absolute configurations of octahedral [M(en)$_3$]Cl_3 complexes (M = Co, Cr, and Rh) by powder X-ray diffraction.[10] Their structural assignments enabled the subsequent elucidation of the absolute configurations of quasiracemates assembled from quasi-mirror-image pairs of these complexes.

Throughout the 1970s, Herpin and co-workers further expanded this field by reporting the crystal structures of [Λ-(+)-Co(en)$_3$·Δ-(–)-Cr(en)$_3$]X_6 (X = Cl or SCN)[11),12)] and [Δ-(+)-Cr(en)$_3$·Λ-(+)-Rh(en)$_3$]X_6, along with racemic Λ/Δ-(±)-[M(en)$_3$]Cl_3 phases.[13] Since these pioneering contributions, a variety of quasiracemate cocrystals incorporating octahedral metal complexes—Ru(II)/Os(II),[14] Fe(II)/Zn(II),[15] Cd(II)/Zn(II),[15] Co(III)/Rh(III),[16] and Co(III)/Cr(III)[17] —as well as square-planar complexes (Ir(I)/Rh(I))[18] have been synthesized and structurally characterized. Despite these advances, broader development of quasiracemate chemistry involving coordination complexes has progressed only sporadically. The inherent complexity of these assemblies—stemming from metal-centered redox chemistry, solubility disparities, and ligand dissociation–association equilibria—has imposed significant experimental constraints, thereby limiting systematic exploration of these promising yet challenging systems.

We previously synthesized square-planar Pd(II) (*S,S*)-**2**[19] and Pt(II) complexes (*S,S*)/(*R,R*)-**3**[20] bearing the optically active Schiff-base ligand (*S*)/(*R*)-**1** (**Fig. 1**), and determined their single-crystal molecular structures. These chiral square-planar complexes exhibit closely analogous molecular geometries and exist in a quasienantiomeric relationship.

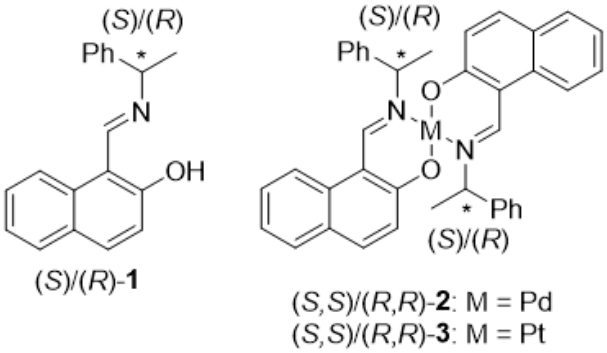

Fig. 1 Molecular structures of chiral ligands (*S*)/(*R*)-**1** and square-planar complexes (*S,S*)/(*R,R*)-**2** and **3**.

In this study, we report the preparation of quasiracemic cocrystals composed of (*S,S*)-**2**/(*R,R*)-**3** or (*R,R*)-**2**/(*S,S*)-**3**, together with their X-ray crystal structures. These structures are directly compared with those of the corresponding racemic crystals of (*S,S*)/(*R,R*)-**2** and (*S,S*)/(*R,R*)-**3**.

2. Experimental

2.1. Preparation of (*R,R*)-2.

The Pd(II) complex (*R,R*)-**2** was prepared from the reaction of (*R*)-**1** with $PdCl_2$ in 70% yield as orange powders, according to the published procedure.[19] The ^{1}H and ^{13}C NMR spectra were consistent with those of (*S,S*)-**2**. Crystallization from CH_2Cl_2/*n*-hexane afforded single crystals suitable for X-ray analysis.

2.2. Preparation of quasiracemic cocrystals, (*S,S*)-2/(*R,R*)-3 and (*R,R*)-2/(*S,S*)-3.

A CH_2Cl_2 solution of (*S,S*)-**2**/(*R,R*)-**3** or (*R,R*)-**2**/(*S,S*)-**3** (1:1 ratio) was added with *n*-hexane at room temperature. Upon slow solvent evaporation, cocrystals of quasiracemates were obtained as red prisms.

2.3. Preparation of racemic crystals of (*S,S*)/(*R,R*)-2 and (*R,R*)/(*S,S*)-3.

Racemic crystals of (*S,S*)/(*R,R*)-**2** were obtained from an equimolar mixture of (*S,S*)-**2** and (*R,R*)-**2** using the same method as for the quasiracemic cocrystals. The

preparation of racemic crystals of (*S,S*)/(*R,R*)-**3** has been reported previously.[20]

2.4. X-ray Analyses.

Crystals suitable for X-ray diffraction were examined using a Rigaku RAXIS-RAPID imaging plate diffractometer (Mo$K\alpha$, λ = 0.71073 Å, graphite monochromator, ω-scan) or a Rigaku XtaLAB mini II benchtop diffractometer equipped with a Mo rotating-anode generator. Structures of the quasiracemic cocrystals (*S,S*)-**2**/(*R,R*)-**3** and (*R,R*)-**2**/(*S,S*)-**3**, and racemic crystals (*S,S*)/(*R,R*)-**2**, and chiral crystals (*R,R*)-**2** were solved using SHELXT[21] or *OLEX*2,[22] and refined by full-matrix least squares on F^2. Non-hydrogen atoms were refined anisotropically. Calculations were performed using *OLEX2*[23] or CrysAlisPro, and ORTEP drawings were generated using ORTEP-3.[24]

Crystallographic data have been deposited with the Cambridge Crystallographic Data Centre as CCDC 2506305 ((*R,R*)-**2**), 2506306 ((*S,S*)-**2**/(*R,R*)-**3**), 2506307 ((*R,R*)-**2**/(*S,S*)-**3**), and 2506308 ((*S,S*)/(*R,R*)-**2**). These data can be obtained free of charge from the CCDC via www.ccdc.cam.ac.uk/data_request/cif, or by emailing data_request@ccdc.cam.ac.uk.

2.5. The Cambridge Structural Database (CSD) Analysis.

The Cambridge Structural Database (CSD, version 6.01, Nov. 2025)[25] was searched for structures corresponding to (*SP*-4-1)-[Pd(*O*^*N*)$_2$] and (*SP*-4-1)-[Pt(*O*^*N*)$_2$] using ConQuest version 2025.3.0.[26] Selected average bond lengths and angles are summarized in **Table 3**.

3. Results and Discussion

When crystals are formed from a solution containing enantiomers, three outcomes are generally possible: racemate crystallization, conglomerate formation, or generation of a solid solution.[27] Racemates are predominant, accounting for approximately 90–95% of cases.[28),29] In the present system, mixtures of the quasienantiomeric pairs (*S,S*)-**2**/(*R,R*)-**3** and (*R,R*)-**2**/(*S,S*)-**3** could, in principle, form conglomerates or solid solutions owing to solubility differences between the Pd(II) and Pt(II) complexes. Nevertheless, slow evaporation from CH_2Cl_2/*n*-hexane reproducibly afforded quasiracemic cocrystals, whose ORTEP drawings are shown in **Figs. 2a** and **2b**. For comparison, **Figs. 2c** and **2d** depict the structures of the corresponding racemic crystals, (*S,S*)/(*R,R*)-**2** and (*S,S*)/(*R,R*)-**3**.

Table 1 summarizes the crystallographic parameters for the quasiracemates and racemates. Both quasiracemic cocrystals crystallize in the monoclinic space group $P2_1$ with Flack parameters of 0.014 and 0.009, confirming the correctness of the assigned absolute structures. With the exception of the β angle of racemic (*S,S*)/(*R,R*)-**2**—which is approximately 3° larger—all lattice constants are essentially comparable.

As shown in **Figs. 2a** and **2b**, the quasiracemates adopt pseudo-enantiomeric arrangements stabilized by $\pi-\pi$ stacking interactions (3.402-3.475 Å) between the naphthalene moieties. Owing to the twofold helical axis of $P2_1$, two pairs of pseudo-enantiomers reside in each unit cell (Z = 2). In contrast, the racemic crystals crystallize in $P2_1/c$ (**2**) and $P2_1/n$ (**3**), space groups related by axis transformation; the presence of the *c*-axis leads to the occurrence of both enantiomers, giving Z = 4. In both racemates, $\pi-\pi$ stacking interactions (3.429-3.442 Å) analogous to those in the quasiracemates are observed

Table 2 lists the coordination bond lengths and angles for the Pd(II) and Pt(II) complexes, while **Table 3** provides averaged values from relevant entries in the CSD (**Fig. 3**). The bond metrics of the quasienantiomeric pairs are consistent with those of structurally related (*SP*-4-1)-[Pd(*O*^*N*)$_2$] and (*SP*-4-1)-[Pt(*O*^*N*)$_2$] complexes reported in the CSD (**Fig. 3**). Although the ionic radius of Pd(II) (66.3 pm) is slightly larger than that of Pt(II) (62.9 pm),[30] this difference (3.4 pm) exerts negligible influence on the chelate geometry.

The four-coordinate geometry index τ_4[31] for all complexes is approximately 0.03, indicating a nearly planar coordination environment with a slight tetrahedral distortion. The O–N–O–N torsion angles define the Δ/Λ helicity at the metal center (**Fig. 4**).[32] As expected, the racemic crystals contain perfect Δ/Λ enantiomeric pairs. In contrast, the Pd(II) and Pt(II) centers within the quasiracemates exhibit opposite helicities, and subtle differences in O–N–O–N torsion angles generate a diastereomeric relationship within the eutectic. The larger τ_4 values observed for **2** relative to **3** suggest that the Pd(II) complexes are more structurally distorted. Notably, τ_4 for **3** in the quasiracemate increases relative to its

Table 1 Crystallographic data for quasiracemic cocrystals, (*R,R*)-**2**/(*S,S*)-**3** and (*S,S*)-**2**/(*R,R*)-**3**, and racemic crystals, (*S,S*)/(*R,R*)-**2** and (*S,S*)/(*R,R*)-**3**

Complex	(*R,R*)-**2**/(*S,S*)-**3**	(*S,S*)-**2**/(*R,R*)-**3**	(*S,S*)/(*R,R*)-**2**	(*S,S*)/(*R,R*)-**3**[a]
Empirical formula	$C_{76}H_{64}N_4O_4PdPt$	$C_{76}H_{64}N_4O_4PdPt$	$C_{38}H_{32}N_2O_2Pd$	$C_{38}H_{32}N_2O_2Pt$
Formula weight	1398.8	1398.8	655.05	743.74
Temperature/K	173.15	173.15	173.15	173.15
Crystal system	monoclinic	monoclinic	monoclinic	monoclinic
Space group	$P2_1$	$P2_1$	$P2_1/c$	$P2_1/n$
a/Å	9.4057(9)	9.4868(4)	9.4793(2)	9.494(2)
b/Å	15.6267(16)	15.6629(7)	15.6520(5)	15.612(4)
c/Å	20.502(2)	20.6265(8)	20.8862(6)	20.663(6)
α/°	90	90	90	90
β/°	100.985(5)	101.3890(10)	104.5370(10)	101.555(12)
γ/°	90	90	90	90
Volume/Å^3	2958.2(5)	3004.6(2)	2999.68(14)	3000.8(14)
Z	2	2	4	4
ρ_{calc} g/cm^3	1.57	1.546	1.450	1.646
μ/mm^{-1}	2.723	2.681	0.656	4.714
F(000)	1408	1408	1344	1472
Crystal size/mm^3	0.26 × 0.23 × 0.22	0.63 × 0.5 × 0.33	0.300 × 0.297 × 0.194	0.34 × 0.18 × 0.16
Radiation	MoK_α (λ = 0.71073)	MoK_α (λ = 0.71073)	MoK_α (λ = 0.71073)	MoK_α (λ = 0.71073)
2θ range for data collection/°	5.986 to 54.966	6.044 to 54.842	6.57 to 54.736	6.578 to 54.898
Index ranges	-11 ≤ *h* ≤ 12 -20 ≤ *k* ≤ 20 -26 ≤ *l* ≤ 26	-12 ≤ *h* ≤ 12 -20 ≤ *k* ≤ 20 -26 ≤ *l* ≤ 26	-11 ≤ *h* ≤ 12 -20 ≤ *k* ≤ 20 -27 ≤ *l* ≤ 26	-11 ≤ *h* ≤ 12 -20 ≤ *k* ≤ 20 -26 ≤ *l* ≤ 26
Reflections collected	28669	28912	28634	27791
Independent reflections	13383 [R_{int} = 0.0451, R_σ = 0.0821]	13493 [R_{int} = 0.0458, R_σ = 0.0820]	6831 [R_{int} = 0.0304, R_σ = 0.0240]	6832 [R_{int} = 0.0886, R_σ = 0.0731]
Data/restraints/parameters	13383/1/779	13492/1/754	6831/0/390	6832/0/390
Goodness-of-fit on F^2	0.958	1.011	1.053	1.062
R_1/wR R_1/wR_2 [$I > 2\sigma(I)$]	0.0288/0.0664	0.0335/0.0742	0.0265/0.0619	0.0498/0.0871
R_1/wR [all data]	0.0341/0.0699	0.0405/0.0783	0.0331/0.0644	0.0720/0.0944
Largest diff. peak/hole / e Å^{-3}	1.27/-1.31	1.18/-1.26	0.41/-0.47	1.63/-1.67
Flack parameter	0.014(3)	0.009(3)	-	-
CCDC No.	2506307	2506306	2506305	1918308

a) See ref. 20.

racemic analogue, approaching the value of **2**—indicating that **3** assumes a geometry more closely resembling the mirror-image configuration of **2**.

4. Conclusion

In conclusion, this study establishes a definitive structural foundation for quasiracemate formation in square-planar complexes by elucidating the quasiracemic cocrystals derived from the quasienantiomeric pairs (*S,S*)-**2**/(*R,R*)-**3** and (*R,R*)-**2**/(*S,S*)-**3**. Single-crystal X-ray diffraction analyses unambiguously reveal that these heterometallic assemblies adopt pseudo-enantiomeric packing architectures that closely emulate those observed in their true racemic counterparts, notwithstanding the intrinsic disparity in metal identity. The quasiracemates crystallize in the chiral space group $P2_1$ with rigorously assigned absolute configurations, whereas the fully racemic analogues manifest in centrosymmetric phases, thereby underscoring the subtle yet consequential interplay between molecular chirality and lattice symmetry.

Comparative structural interrogation demonstrates that both the Pd(II) and Pt(II) complexes preserve coordination metrics that align with established (*SP*-4-1)-[M(*O*^*N*)$_2$] structure documented in the CSD. The

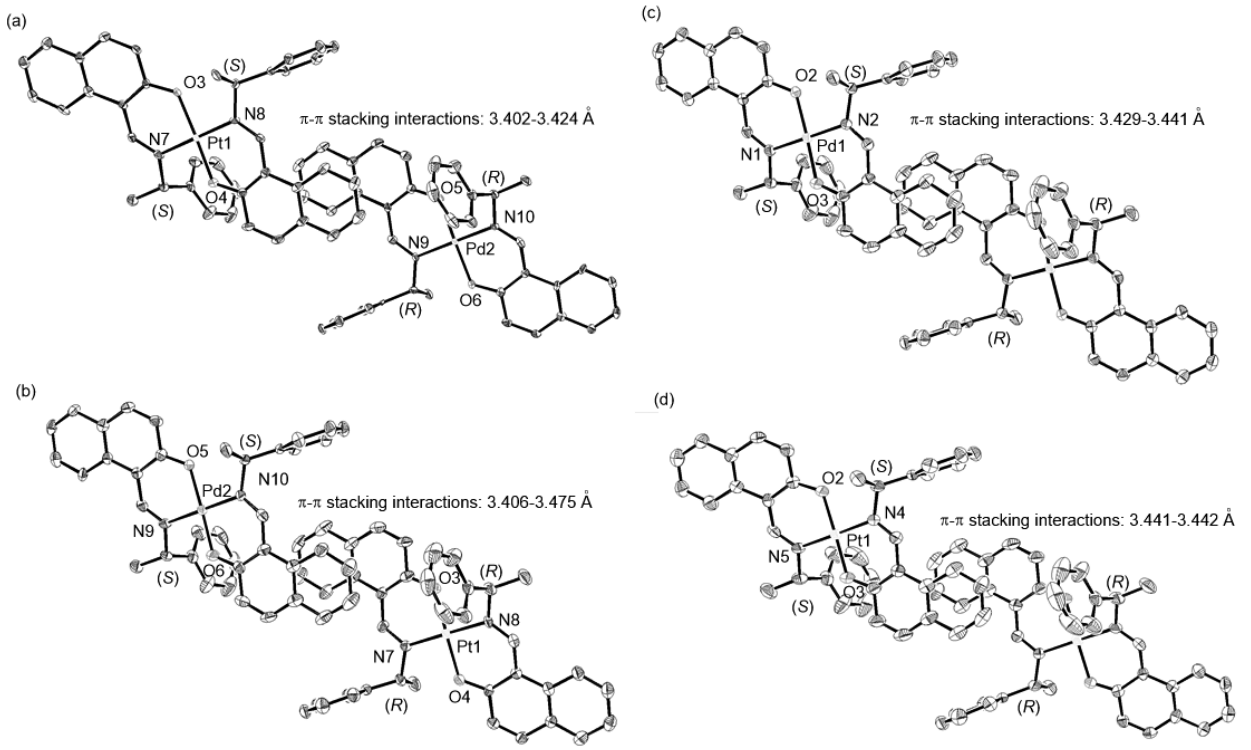

Fig. 2 ORTEP drawings for quasiracemic cocrystals of (*S,S*)-**2**/(*R,R*)-**3** (a) and (*R,R*)-**2**/(*S,S*)-**3** (b), and for racemic crystals of (*S,S*)/(*R,R*)-**2** (c) and (*S,S*)/(*R,R*)-**3** (d). Hydrogen atoms are omitted for clarity.

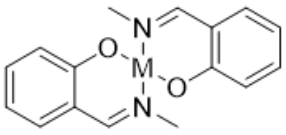

(*SP*-4-1)-[M(*O*^*N*)$_2$]
M = Pd or Pt

Fig. 3 Structures of (*SP*-4-1)-[Pd(*O*^*N*)$_2$] and (*SP*-4-1)-[Pt(*O*^*N*)$_2$] in the CSD searches.

Fig. 4 Helical orientation of O–N chelate axes defining *Δ*/*Λ* chirality (bold line front, dashed line rear).

marginal difference in ionic radii between Pd(II) and Pt (II) exerts only a minimal influence on the chelate geometry. Nonetheless, nuanced modulations in O–N–O–N torsion angles impart a diastereomeric relationship between the metal centers within the quasiracemates, in contrast to the symmetry-mandated *Δ*/*Λ* pairs of the racemates. Particularly noteworthy is the enhanced tetrahedral distortion in Pt(II) complex **3** within the quasiracemate lattice, which converges toward that of the Pd(II) congener **2**, highlighting the structural malleability requisite for achieving quasi-mirror-image packing.

Collectively, these findings provide a rare and incisive comparison between racemic and quasiracemic architectures in coordination chemistry and illuminate fundamental principles governing the assembly of quasi-enantiomeric metal–ligand frameworks. Beyond their structural significance, the results delineate new conceptual guidelines for the deliberate construction of heterometallic chiral solids, thereby opening avenues for the rational design of functional materials whose properties derive from controlled quasiracemic organization.

Acknowledgements

This work was supported by JSPS KAKENHI (Grant Numbers JP23K13768 (M.I.), JP21K05234 (T.T.), and JP25K08599 (T.T.)), foundation for the promotion of ion

Table 2 Selected bond lengths (Å), angles (deg), torsion angles (deg), and four-coordinate geometry index (τ_4)[a,b] for quasiracemic cocrystals, (*R,R*)-**2**/(*S,S*)-**3** and (*S,S*)-**2**/(*R,R*)-**3**, and racemic crystals, (*S,S*)/(*R,R*)-**2** and (*S,S*)/(*R,R*)-**3**

(*R,R*)-**2**/(*S,S*)-**3**		(*S,S*)-**2**/(*R,R*)-**3**		(*S,S*)/(*R,R*)-**2**		(*S,S*)/(*R,R*)-**3**[c]	
Bond lengths							
Pd2-O5	1.973(4)	Pd2-O5	1.985(5)	Pd1-O2	1.9835(13)		
Pd2-O6	1.983(4)	Pd2-O6	1.982(5)	Pd1-O3	1.9751(13)		
Pd2-N9	2.019(5)	Pd2-N9	2.036(7)	Pd1-N1	2.0193(15)		
Pd2-N10	2.024(5)	Pd2-N10	2.028(6)	Pd1-N2	2.0287(16)		
Pt1-O3	1.991(4)	Pt1-O3	1.978(5)			Pt1-O2	1.992(4)
Pt1-O4	1.974(4)	Pt1-O4	1.997(5)			Pt1-O3	1.979(4)
Pt1-N7	2.024(5)	Pt1-N7	1.990(6)			Pt1-N4	2.009(5)
Pt1-N8	2.002(5)	Pt1-N8	2.017(6)			Pt1-N5	2.016(5)
Bond angles							
O5-Pd2-N9	91.52(18)	O5-Pd2-N9	89.6(2)	O2-Pd1-N1	89.95(6)		
O5-Pd2-N10	89.09(19)	O5-Pd2-N10	89.8(2)	O2-Pd1-N2	89.60(6)		
O6-Pd2-N9	89.24(18)	O6-Pd2-N9	89.5(2)	O3-Pd1-N1	91.33(6)		
O6-Pd2-N10	90.23(19)	O6-Pd2-N10	91.2(2)	O3-Pd1-N2	89.19(6)		
O5-Pd2-O6	177.24(16)	O5-Pd2-O6	177.3(2)	O2-Pd1-O3	177.42(6)		
N9-Pd2-N10	178.06(18)	N9-Pd2-N10	178.1(3)	N1-Pd1-N2	178.09(6)		
O3-Pt1-N7	90.67(19)	O3-Pt1-N7	92.4(2)			O2-Pt1-N4	88.81(19)
O3-Pt1-N8	89.05(17)	O3-Pt1-N8	88.3(2)			O2-Pt1-N5	90.76(19)
O4-Pt1-N8	92.03(18)	O4-Pt1-N8	90.9(2)			O3-Pt1-N4	91.8(2)
O4-Pt1-N7	88.33(19)	O4-Pt1-N7	88.4(2)			O3-Pt1-N5	88.7(2)
O3-Pt1-O4	177.47(16)	O3-Pt1-O4	177.5(2)			O2-Pt1-O3	178.06(19)
N7-Pt1-N8	178.11(19)	N7-Pt1-N8	178.3(3)			N4-Pt1-N5	178.0(2)
Torsion angles							
O5-N9-O6-N10	3.16 (*Δ*)	O5-N9-O6-N10	-3.02 (*Λ*)	O2-N1-O3-N2	±3.00 (*Δ*/*Λ*)		
O3-N7-O4-N8	-2.89 (*Λ*)	O3-N7-O4-N8	2.68 (*Δ*)			O2-N4-O3-N5	±2.65 (*Δ*/*Λ*)
Four-coordinate geometry index τ_4							
0.033 for (*R,R*)-**2**		0.033 for (*S,S*)-**2**			0.032		
0.031 for (*S,S*)-**3**		0.030 for (*R,R*)-**3**					0.028

a) $\tau_4 = (360° - (\alpha + \beta))/141$, α = O-M-O, β = N-M-N. b) see ref. 31. c) see ref. 20.

Table 3 Average bond lengths (Å) and average bond angles (deg), and average torsion angles (deg) of (*SP*-4-1)-[Pd(*O^N*)$_2$] and [Pt(*O^N*)$_2$] complexes in CSD[a]

Complex	Average bond lengths[b]	Average bond angles[b]	Average torsion angle[b,c]
(*SP*-4-1)-[Pd(*O^N*)$_2$][d]	Pd-N 2.019 (0.020), Pd-O 1.983 (0.012)	O-Pd-N 91.27 (1.52),[e] O-Pd-N 88.77 (1.59),[f] O-Pd-O 178.66 (2.28), N-Pd-N 178.60 (2.17)	O-N-O-N 1.75 (99 complexes have 0°)
(*SP*-4-1)-[Pt(*O^N*)$_2$][g]	Pt-N 2.011 (0.015), Pt-O 1.993 (0.015)	O-Pt-N 92.28 (0.91),[e] O-Pt-N 87.85 (0.99),[f] O-Pt-O 177.12 (2.20), N-Pt-N 177.70 (3.08)	O-N-O-N 4.04 (18 complexes have 0°)

a) CSD ver. 6.01 (Nov. 2025) was used. b) The numbers in parentheses are standard deviations. c) Absolute average values. d) 174 data for (*SP*-4-1)-[Pd(*O^N*)$_2$]. e) Bond angles formed by one *O^N* ligand. f) Bond angles formed by two *O^N* ligands . g) 125 data for (*SP*-4-1)-[Pt(*O^N*)$_2$].

engineering (M.I.), and Izumi Science and Technology Foundation (grant number 2025-J-037 (M.I.)). We gratefully acknowledge Prof. Dr. Henri Brunner (Universität Regensburg) for helpful discussion and comments. Our gratitude goes to the Cambridge Crystallographic Data Centre (CCDC) for providing the necessary data for the complexes (*SP*-4-1)-[Pd(*O^N*)$_2$] and (*SP*-4-1)-[Pt(*O^N*)$_2$] in Table 3.

References

1) For reviews, see: X. Wang, Z. Wang, X. Wang, F. Kang, Q. Gu, Q. Zhang, Recent Advances of Organic Cocrystals in Emerging Cutting-Edge Properties and Applications, *Angew. Chem. Int. Ed.* **2024**, *63*, e202416181; S. Aitipamula, G. Bolla, Optimizing Drug Development: Harnessing the Sustainability of Pharmaceutical Cocrystals, *Mol. Pharam.* **2024**, *21*, 3121 − 3143; G. Bolla, B. Sarma, A. K. Nangia, Crystal Engineering of Pharmaceutical Cocrystals in the Discovery and Development of Improved Drugs, *Chem. Rev.* **2022**, *122*, 11514 − 11603; A. Alvani, A. Shayanfar,

Solution Stability of Pharmaceutical Cocrystals, *Cryst. Growth Des.* **2022**, *22*, 6323 − 6337; R. Rathi, S. Kaur, I. Singh, A Review on Co-crystals of Herbal Bioactives for Solubility Enhancement: Preparation Methods and Characterization Techniques, *Cryst. Growth Des.* **2022**, *22*, 2023 − 2042; W. Heng, X. He, Y. Song, J. Han, Z. Pang, S. Qian, J. Zhang, Y. Gao, Y. Wei, Insights into Cocrystallization and Coamorphization Engineering Techniques in the Delivery of Traditional Chinese Medicine: Formation Mechanism, Solid-State Characterization, and Improved Pharmaceutical Properties, *Cryst. Growth Des.* **2022**, *22,* 5110 − 5134.

2） Q. Zhang, A. Rivkin, D. P. Curran, Quasiracemic Synthesis: Concepts and Implementation with a Fluorous Tagging Strategy to Make Both Enantiomers of Pyridovericin and Mappicine, *J. Am. Chem. Soc.* **2002**, *124*, 5774 − 5781; Q. Zhang, D. P. Curran, Quasienantiomers and Quasiracemates: New Tools for Identification, Analysis, Separation, and Synthesis of Enantiomers, *Chem. Eur. J.* **2005**, *11*, 4866 − 4880; S. P. Kelley, L. Fábián, C. P. Brock, Failures of fractional crystallization: ordered co-crystals of isomers and near isomers, *Acta Crystallogr., Sect. B* **2011**, *B67*, 79 − 93.

3） M. S. Hendi, R. E. Davis, V. M. Lynch, K. A. Wheeler, Structural studies of enantiomers, racemates, and quasiracemates. 2-(2,4-dichlorophenyl)propanoic acid and 2-(2-chloro-4-nitrophenyl)propanoic acid, *Cryst. Eng.* **2001**, *4*, 11 − 24; S. L. Fomulu, M. S. Hendi, R. E. Davis, K. A. Wheeler, Structural Studies of Enantiomers, Racemates, and Quasiracemates. 2-(2,4,5-Trichloroanilino)propanoic Acid and 2-(2,4,5-Trichlorophenoxy)propanoic Acid, *Cryst. Growth Des.* **2002**, *2*, 637 − 644; M. S. Hendi, P. Hooter, R. E. Davis, V. M. Lynch, K. A. Wheeler, Structural Studies of Enantiomers, Racemates, and Quasiracemates: *N*-(4-Methylbenzoyl) methylbenzylamine and *N*-(4-Nitrobenzoyl) methylbenzylamine, *Cryst. Growth Des.* **2004**, *4*, 95 − 101; A. M. Lineberry, E. T. Benjamin, R. E. Davis, W. S. Kassel, K. A. Wheeler, Structural Studies of Racemates and Quasiracemates: Chloro, Bromo, and Methyl Adducts of 2-Phenoxypropionic Acid, *Cryst. Growth Des.* **2008**, *8*, 612 − 619; R. C. Grove, S. H. Malehorn, M. E. Breen, K. A. Wheeler, A photoreactive crystalline quasiracemate, *Chem. Commun.* **2010**, *46*, 7322 − 7324; K. A. Wheeler, R. C. Grove, R. E. Davis, W. S. Kassel, Rediscovering Pasteur's Quasiracemates, *Angew. Chem. Int. Ed.* **2008**, *47*, 78 − 81; Y. Lu, A. J. Bolokowicz, S. A. Reeb, J. D. Wiseman, K. A. Wheeler, Chiral transmission to crystal photodimerizations of leucine–methionine quasiracemic assemblies, *RSC Adv.* **2014**, *4*, 8125 − 8131; C. H. Görbitz, P. Karen, Twin Displacive Phase Transitions in Amino Acid Quasiracemates, *J. Phys. Chem. B* **2015**, *119*, 4975 − 4984; G. Lautrette, B. Kauffmann, Y. Ferrand, C. Aube, N. Chandramouli, D. Dubreuil, I. Huc, *Angew. Chem. Int. Ed.* **2013**, *52*, 11517 − 11520; C. H. Görbitz, D. S. Wragg, I. M. B. Bakke, C. Fleischer, G. Grønnevik, M. Mykland, Y. Park, K. W. Trovik, H. Serigstad, B. E. V. Sundsli, A phase transition from monoclinic *C*2 with $Z' = 1$ to triclinic *P*1 with $Z' = 4$ for the quasiracemate L-2-aminobutyric acid–D-methionine (1/1), *Acta Crystallogr., Sect. C* **2016**, *C72*, 536 − 543; J. M. Spaniol, K. A. Wheeler, Accessing Centnerszwer's quasiracemate molecular shape controlled molecular recognition, *RSC Adv.* **2016**, *6*, 64921 − 64929; M. M. H. Smets, E. Kalkman, P. Tinnemans, A. M. Krieger, H. Meekes, H. M. Cuppen, Increasing the Structural Boundary of Quasiracemate Formation: 4-Substituted Naphthylamides, *CrystEngComm* **2017**, *19*, 5604 − 5610; I. C. Tinsley, J. M. Spaniol, K. A. Wheeler, Mapping the structural boundaries of quasiracemate fractional crystallization using 2-substituted diarylamides, *Chem. Commun.* **2017**, *53*, 4601 − 4604; E. N. Pinter, L. S. Cantrell, G. M. Day, K. A. Wheeler, Pasteur's tartaramide/malamide quasiracemates: new entries and departures from near inversion symmetry, *CrystEngComm* **2018**, *20*, 4213 − 4220; R. G. Wells, K. D. Sahlstrom, F. I. Ekelem, K. A. Wheeler, Amino acid hydrogen oxalate quasiracemates – hydrocarbon side chains, *CrystEngComm* **2021**, *23*, 8053 − 8060; X. Wu, J. Malinčík, A. Prescimone, C. Sparr, X-Ray Crystallographic Studies of Quasi-Racemates for Absolute Configuration Determinations, *Helv. Chim.*

Acta **2022**, *105*, e202200117.

4）S. Yang, Y. Li, F. Kang, F. Li, S. Zhao, Y. Sun, C. Zhang, Q. Zhang, Recent Progress in Organic Cocrystal-Based Superlattices and Their Optoelectronic Applications, *Adv. Funct. Mater.* **2025**, *35*, 2504976; X. Wang, Z. Wang, X Wang, F. Kang, Q. Gu, Q. Zhang, Recent Advances of Organic Cocrystals in Emerging Cutting-Edge Properties and Applications, *Angew. Chem. Int. Ed.* **2024**, *63*, e202416181; M. Singh, K. Liu, S. Qu, H. Ma, H. Shi, Z. An, W. Huang, Recent Advances of Cocrystals with Room Temperature Phosphorescence, *Adv. Optical Mater.* **2021**, *9*, 2002197.

5）C. Zhang, X. Wang, Y. Li, Y. Sun, Q. Zhang, Spin in Organic Cocrystals, *Chem. Eur. J.* **2023**, *29*, e202300481; M. Jiang, C. Zhen, S. Li, X. Zhang, W. Hu, Organic Cocrystals: Recent Advances and Perspectives for Electronic and Magnetic Applications, *Front. Chem.* **2021**, *9*, 764628.

6）G. Liu, S.-H. Wei, C. Zhang, Review of the Intermolecular Interactions in Energetic Molecular Cocrystals, *Cryst. Growth Des.* **2020**, *20*, 7065 − 7079; J. C. Bennion, A. J. Matzger, Development and Evolution of Energetic Cocrystals, *Acc. Chem. Res.* **2021**, *54*, 1699 − 1710.

7）S. Ito, K. Fukuhara, N. Arakawa, S. Suzuki, Y. Imai, Quasiracemic Crystallization of Luminescent Chiral Molecules: Mechanochromic Luminescence and Sign Inversion of Circularly Polarized Luminescence, *Chem. Eur. J.* **2025,** *31*, e202501677.

8）M. M. Delépine, Sur les racémiques actifs, *Bull. Soc. Chim. Fr.* **1921**, *29*, 656 − 669.

9）M. M. Delépine, B. Charonnat, Utilisation des racémiques actifs pour la determination de la configuration d'homéomères: Application aux sels de cobalt-III et de rhodium-III tri-éthylène-diamine optiquement actifs, *Bull. Soc. Fr. Mineralogie* **1930**, *53*, 73 − 84.

10）P. Andersen, F. Galsbøl, S. E. Harnung, Correlation of the Absolute Configurations of Tris(diamine) complexes by Means of X-ray Powder Photographs of Active Racemates, *Acta Chim. Scand.* **1969**, *23*, 3027 − 3037.

11）A. Whuler, C. Brouty, M. P. Spinat, P. Herpin, Étude préliminaire des mailles cristallines des chlorues racémiwues et racémique actif de cobalt(III) et de chrom(III) triéthylènediamine, hydrates, *C. R. Acad. Sc. Paris C* **1975**, *280*, 1097 − 1099; A. Whuler, C. Brouty, P. Spinat, P. Herpin, Etude structurale du complexe racémique actif hydraté $[(+)\text{-}Coen_3(-)\text{-}Cren_3]Cl_6.6,1H_2O$, *Acta Crystallogr., Sect. B* **1976**, *B32*, 194 − 198.

12）C. Brouty, P. Spinat, A. Whuler, P. Herpin, Synthèse et caractérisation du complexe « racémique actif » $[(+)Co(en)_3(-)Cr(en)_3](SCN)_6, nH_2O$, *Bull. Soc. Fr. Mineral. Crystal.* **1975**, *98*, 218 − 222; C. Brouty, P. Spinat, A. Whuler, P. Herpin, Détermination structurale à 293 et 133 K du complexe racémique actif $[(+)\text{-}Co(en)_3(-)Cr(en)_3](SCN)_6.nH_2O$, *Acta Crystallogr., Sect. B* **1977**, *B33*, 2563 − 2572.

13）A. Whuler, C. Brouty, P. Spinat, P. Herpin, Le complexe racémique actif $[(+)\text{-}Cren_3(+)\text{-}Rhen_3]Cl_6.6H_2O$, *Acta Crystallogr., Sect. B* **1976**, *B32*, 2542 − 2544; A. Whuler, C. Brouty, M. P. Spinat, P. Herpin, Étude cristallographique des chlorures de rhodium(III) triethylenediamine, hydrates, sous forms active, racémique et racémique active, *C. R. Acad. Sc. Paris C* **1977**, *284*, 117 − 119.

14）J. Breu, C. Kratzer, H. Yersin, Crystal Engineering as a Tool for Directed Radiationless Energy Transfer in Layered $\{\Lambda\text{-}[Ru(bpy)_3]\Lambda\text{-}[Os(bpy)_3]\}(PF_6)_4$, *J. Am. Chem. Soc.* **2000**, *122*, 2548 − 2555.

15）Y. Popowski, I. Goldberg, M. Kol, Assembling Quasi-enantiomeric Octahedral Complexes of Different Metals via Quasi-racemate Crystallization, *Chem. Eur. J.* **2016**, *22*, 5530 − 5533.

16）R. Kuroda, Chiral discriminations and crystal packing. Two diastereomeric compounds involving complex ions of D_3 symmetry, [tris(ethylenediamine)cobalt(III)] and [tris(oxalato)rhodate(III)], *Inorg. Chem.* **1991**, *30*, 4954 − 4959.

17）I. Kalf, B. Calmuschi, U. Englert, Chiral Cr(III) and Co(III) complex cations as building blocks for ordered and disordered salts, *CrystEngComm* **2002**, *49*, 548 − 551.

18）V. Schurig, W. Pille, W. Winter, Construction of an Alternating (Rh, Rh, Ir, Ir)$_\infty$-Columnar Structure via a Quasiracemate, *Angew. Chem. Int. Ed. Engl.* **1983**, *22*, 327 − 328.

19）H. Brunner, H. Iwabe, T. Tsuno, Synthesis and structural characterization of isomeric palladium(II)

complexes with chiral *N,O*-bidentate ligands, *Inorg. Chim. Acta* **2013**, *400*, 262 − 266.

20) M. Ikeshita, S. Furukawa, T. Ishikawa, K. Matsudaira, Y. Imai, T. Tsuno, Enhancement of Chiroptical Responses of *trans*-Bis[β-iminomethyl) naphthoxy]platinum(II) Complexes with Distorted Square Planar Coordination Geometry, *ChemistryOpen* **2022**, *11*, e202100277.

21) G. M. Sheldrick, SHELXT – Integrated space-group and crystal-structure determination, *Acta Crstallogr., Sect. A* **2015**, *A71*, 3 − 8.

22) L. J. Bourhis, O. V. Dolomanov, R. J. Gildea, J. A. K. Howard, H. Puschmann, The anatomy of a comprehensive constrained, restrained refinement program for the modern computing environment – *Olex2* dissected, *Acta Crstallogr., Sect. A* **2015**, *A71*, 59 − 75.

23) O. V. Dolomanov, L. J. Bourhis, R. J. Gildea, J. A. K. Howard, H. Puschmann, *OLEX2*: a complete structure solution, refinement and analysis program, *J. Appl. Crystrallogr.* **2009**, *42*, 339 − 341.

24) M. N. Burnett, C. K. Johnson, "ORTEP-III: Oak Ridge Thermal Ellipsoid PlotProgram for Crystal Structure Illustrations," Report ORNL-6895, Oak Ridge National Laboratory, Oak Ridge, 1996.

25) C. R. Groom, I. J. Bruno, M. P. Lightfoot, S. C. Ward, New software for searching the Cambridge Structural Database and visualizing crystal structures, *Acta Crystallogr., Sect. B* **2016**, *B72*, 171 − 179.

26) J. C. Cole, P. R. Edgington, M. Kessler, C. F. Macrae, P. McCabe, J. Pearson, R. Taylor, New software for searching the Cambridge Structural Database and visualizing crystal structures, *Acta Crystallogr., Sect. B* **2002**, *B58*, 389 − 397.

27) E. L. Eliel, S. H. Wilen, Stereochemistry of Organic Compounds, Wiley, New York, 1994.

28) J. Jacques, M. Leclercq, M.-J. Brienne, La formation de sels augmente-t-elle la fréquence des dédoublements spontanés?, *Tetrahedron* **1981**, *37*, 1727 − 1733.

29) C. J. Welch, Formation of highly enantioenriched microenvironments by stochastic sorting of conglomerate crystals: A plausible mechanism for generation of enantioenrichment on the prebiotic earth, *Chirality* **2001**, *13*, 425 − 427.

30) M. Alsalmana, Y. A. Alghofaili, A. A.B. Baloch, H. Alsadah, A. A. Alsaui, S. M. Alqahtani, A. H. Muqaibel, F. H. Alharbi, Outliers in Shannon's effective ionic radii table and the table extension by machine learning, *Comp. Mater. Sci.* **2023**, *228*, 112350.

31) L. Yang, D. R. Powell, R. P. Houser, Structural variation in copper(i) complexes with pyridylmethylamide ligands: structural analysis with a new four-coordinate geometry index, τ_4, *Dalton Trans.* **2007**, 955 − 964.

32) H. Brunner, M. Bodensteiner, T. Tsuno, Chirality in Distorted Square Planar Pd(*O,N*) Compounds, *Chirality* **2013**, *25*, 663 − 667.

光学活性 Schiff 塩基配位子を伴った Pt(II) 錯体と Pd(II) 錯体との準ラセミ共結晶

池下　雅広，津野　孝

概　　要

キラル金属錯体の準エナンチオマー対から形成される準ラセミ化合物は，分子のキラリティーと固体状態のパッキングとの関係を調査するためのプラットフォームを提供する。本研究では，光学活性シッフ塩基配位子を有する平面四角形 Pd(II) および Pt(II) 錯体 (*S,S*)-**2**/(*R,R*)-**3** および (*R,R*)-**2**/(*S,S*)-**3** からなる準ラセミ共結晶の合成と単結晶 X 線構造解析について報告する。CH_2Cl_2/ ヘキサン溶液からの低速溶媒蒸発により赤色プリズムが得られ，キラル空間群 $P2_1$ とする絶対配置で結晶化した。一方，(*S,S*)/(*R,R*)-**2** および (*R,R*)/(*S,S*)-**3** のラセミ結晶は中心対称配置 ($P2_1/c$, $P2_1/n$) をとる。構造解析により，配位子間の $\pi-\pi$ 相互作用によって安定化された擬似エナンチオマーパッキングが明らかになり，金属中心が異なるにもかかわらず，ラセミ体の配置を厳密に模倣する。配位構造はケンブリッジ構造データベースの (*SP*-4-1)-[M(*O*^*N*)$_2$] (M = Pd, Pt) と一致しており，Pd(II) と Pt(II) のイオン半径の差はキレート骨格にほとんど影響を与えない。O–N–O–N ねじれ角の微妙な変化は，準ラセミ体内部にジアステレオマー関係をもたらし，準鏡像パッキングに必要な構造適応性を反映している。本研究は，平面四角形金属錯体のラセミ体と準ラセミ体の集合体間の稀有かつ厳密な比較を提供し，制御された格子対称性と潜在的な機能特性を有するヘテロ金属キラル固体の設計指針を確立する。

Biographical Sketches of the Authors

Masahiro Ikeshita completed his undergraduate study at Kansai University in 2016 under the supervision of Prof. Yutaka Nishiyama and Prof. Rui Umeda. He subsequently received his Master's degree and Ph.D. degree in 2018 and 2021, respectively, under the supervision of Prof. Takeshi Naota at Osaka University. He was appointed Assistant in the College of Industrial Technology, Department of Applied Molecular Chemistry at Nihon University in 2021 and was promoted to an Assistant Professor in 2023. His research focused on design, synthesis, and development of functional molecular materials based on coordination chemistry and organic synthesis.

Takashi Tsuno obtained his Ph.D. in 2005 from the University of Shizuoka under supervision of Professor Masayuki Sato and his *Dr. rer. nat.* from the University of Regensburg in 2007 under supervision of Professor Henri Brunner. He is a Professor at Nihon University since 2010. His research interests include synthesis and stereochemistry of chiral-at-metal compounds.